

The COMPASS sandwich veto detector and a first look at kaonic final states from a π^- (190 GeV) beam on a proton target

Tobias Schlüter^a for the COMPASS collaboration

LMU Munich

Abstract. We introduce the sandwich veto detector that was built for the 2008 and 2009 hadron runs of the COMPASS experiment at CERN. During these beamtimes it was serving as a veto detector for neutral and charged particles outside the spectrometer acceptance, mostly thought to originate from reactions which excited the target. We also present first mass spectra from π^- (190 GeV) $p \rightarrow \pi^- K_S^0 K_S^0 p$ that were measured in the 2008 hadron run.

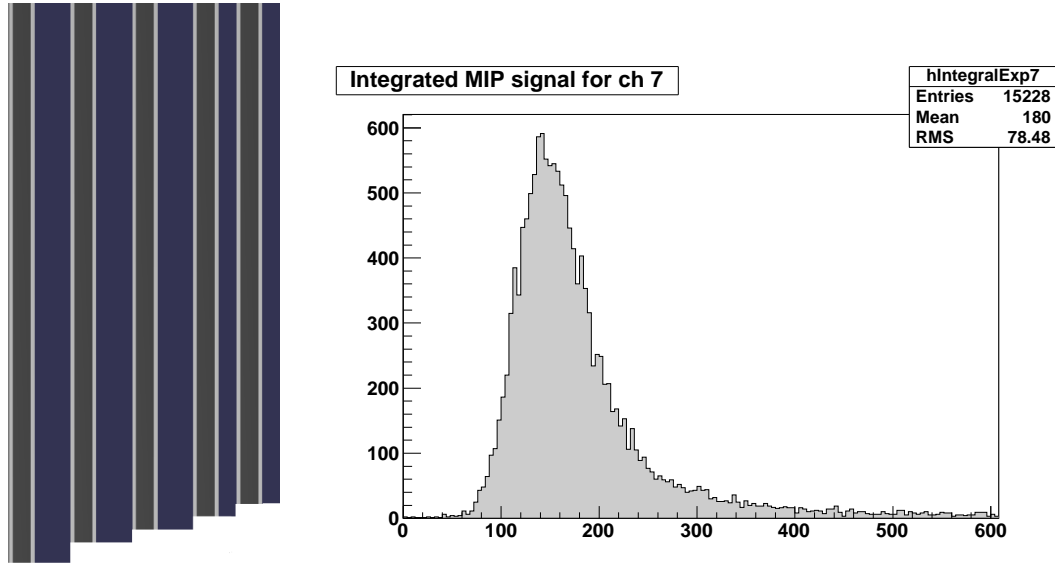
1 Introduction

The COMPASS experiment at CERN is a multi-purpose, two-stage spectrometer pursuing a variety of fixed-target physics programmes [1]. Its 2008 and 2009 Pion runs were dedicated to studying mesonic states produced both as diffractive excitations of the scattered beam pion and as objects produced centrally between the scattered beam pion and the recoiling proton target. In order to suppress events with particles lying outside the spectrometer acceptance, the sandwich veto detector was installed between the target recoil detector [2] and the spectrometer. The design of the detector and its performance in the 2008 pion run are discussed in sec. 2. As an illustration of both the performance of the COMPASS spectrometer as a whole and the current status of our analyses, we present some preliminary results concerning neutral kaonic final states in sec. 3 and discuss the prospects for partial wave analyses of those states.

2 The Sandwich Veto Detector

The acceptance of the COMPASS spectrometer as seen from the target is approximately conical with the beam direction along the symmetry axis of the cone and an opening angle of the cone of 11 degrees as seen from the center of the liquid hydrogen target. The recoil proton detector (RPD) covers angles above 55 degrees. In order to reject events where a particle ends up between these two acceptances, a veto detector had to be placed between the RPD and the spectrometer. Since it had to detect both charged (mostly pions) and neutral particles (mostly photons from neutral pion decays), a thin electromagnetic calorimeter was designed for this purpose, the sandwich veto detector. The design criteria differed from an electromagnetic calorimeter as found e.g. in both of the stages of the COMPASS spectrometer insofar, as energy resolution (and therefore good shower containment, high radiation length) could be sacrificed in order to allow for fast readout and the little space available in the direction along the beam direction. Likewise, spatial resolution was not a requirement in the design. On the other hand, high detection efficiency for low-energetic photons was required, extending below 100 MeV together with high rate capability.

^a e-mail: tobias.schlueter@physik.uni-muenchen.de



(a) Schematic cross section of a module. Lead is depicted in dark gray, steel in light gray, scintillators in blue. Target to the left, spectrometer to the right. The step structure near the bottom indicates the shape chosen to match the spectrometer acceptance.

(b) MIP response. The picture shows the integrated response of one PMT as recorded by the SADC readout for events where a muon hit the corresponding detector module. The axes are labelled in arbitrary units. The distribution is broadened from the expected Landau distribution due to statistical fluctuations of the light collection. The clear separation from zero is indicative of the high efficiency.

Fig. 1: Design and performance of the sandwich veto detector.

In order to achieve these goals, the following design was settled upon: the $2 \times 2 \text{ m}^2$ active surface of the detector was divided into 12 modules, each read out by 208 optically active wavelength shifting optical fibres converging on a single photomultiplier. A central hole, corresponding to the spectrometer acceptance, was left empty. Each module consists of a sandwich of five lead layers alternating with plastic scintillators. Each lead layer has steel plates glued to it on both sides in order to ensure mechanical stability. The design is illustrated in fig. 1a. In order to economize in thickness, the two most downstream scintillator layers are implemented at half thickness, compared to the other layers' thickness of 10 mm. This choice was made after confirming in Monte Carlo that this combination gives the best efficiency for low-energy photons. The lead layers are 5 mm each, the steel layers 1 mm. The optical fibres are glued into grooves cut into the scintillators.

With this setup we estimated nearly perfect detection efficiency for minimum ionizing particles (MIPs), while being only slightly susceptible to false vetoes from δ -electron irradiation. These predictions were confirmed in the course of the experiment. COMPASS uses a wide high-energy muon beam for alignment that illuminates most of the surface of the sandwich detector. Using this beam, we confirmed a MIP detection efficiency of $> 98\%$ after accounting for inefficiencies along the edges of the individual detector modules by comparing hits predicted from COMPASS's tracking with actual hits recorded in the sandwich veto detector. This degree of efficiency, together with the electronic thresholds used for the veto signal lead – by comparison with our Monte Carlo studies of energy deposits – to an efficiency of $> 70\%$ for 100 MeV photons. Photon energy deposits increase steeply with increasing photon energy, as does the detection efficiency.

Comparing the trigger rates for various triggers in the COMPASS experiment with and without the sandwich veto detector included in the triggers leads to the following figures of merit:

1. enrichment factor 3.2: the trigger rates for the main physics trigger DT0 increase by a factor 3.2 if the sandwich is not included in the veto.
2. false vetoes happen for about 2% of all events. This lies within Monte Carlo expectations for rates induced by δ -electrons, and has been verified in different physics scenarios.
3. the performance of the detector doesn't seem to suffer from the increased rates during the 2009 run.

Ongoing studies of the sandwich veto concern its light collection efficiency and a detailed understanding of its geometrical acceptance. After the 2009 run of the experiment it was removed from the experimental area as it is not needed for the COMPASS muon run that is going to take place in 2010.

3 A first look at kaonic final states

3.1 Motivation

Data collected in the 190 GeV/c π^-p run of 2008 allow high statistics studies of kaonic channels in diffractive and central processes. It is useful to remember the allowed quantum number combinations of neutral $K\bar{K}$ systems (all with isospin $I = 0$ or 1):

state	allowed J^{PC}				
$K_S^0 K_S^0$	0^{++}	2^{++}	4^{++}		
$K_S^0 K_L^0$		1^{--}	3^{--}		
$K^+ K^-$	0^{++}	1^{--}	2^{++}	3^{--}	4^{++}

Previous work on the centrally produced $K^+ K^-$ system at 450 GeV/c by WA102 resulted in a $q\bar{q}$ ($q = u, d, s$) and glueball mixing scheme for the 0^{++} states observed at 980, 1370, 1500, and 1710 MeV/c² [3,4,5]. Open questions concern the resonance nature of $f_0(1370)$, with inconsistent decay branchings in other production processes [6,7], and the extension of the level scheme to the 2 GeV/c² region, in particular for the 0^{++} and 2^{++} states which are the quantum numbers of the lightest expected glueballs.

Preferential $K\bar{K}$ decay of glueballs was recently predicted on the basis of chirality arguments, in contrast to earlier expectations of flavour blind decay [8]. The $K_S^0 K_S^0$ ($K_S^0 K_L^0$) system is particularly suited for spectroscopy because of its selectivity for $C = +$ ($-$) states. From previous central production studies, only poor statistics data exist on $K_S^0 K_S^0$. COMPASS data outdo these by more than an order of magnitude and are virtually free of background, but at the price of no clear separation between diffractively and centrally produced final states.

The $K\bar{K}\pi$ system, as produced in diffractive π^-p collisions, can exist with exotic quantum numbers 1^{-+} . Preferential $K^*(\rightarrow K\pi)K$ decay is expected from models of quartet and hybrid states [9,10]. So far no kaonic exotics emerged from various experimentally studied production processes [7]. Since their existence is inevitable in flavour multiplet schemes, they can be considered as touchstones of quartet models. COMPASS produced $K_S^0 K_S^0 \pi^-$ with high statistics, well suited for partial wave analysis. In addition to exotics, states or dublets with $q\bar{q}$ quantum numbers like the enigmatic $E/i(1405)$ or $\pi(1800)$ will possibly make an appearance in these data.

In order to disentangle the angular distributions of the final states, and thereby the physical content, partial wave analysis needs to be performed. For this we will make use of two software packages that are currently being developed within our collaboration.

At this conference we give a first impression of the status of our analysis of the $K_S^0 K_S^0$ channel, but analyses of the sibling $K^+ K^-$ and $K_L^0 K_S^0$ channels are also underway. The $K_S^0 K_S^0$ channel is the easiest of these in terms of selection, as the two displaced vertices of the preferred K_S^0 decay into a pair of charged pions are a fairly unique signature.

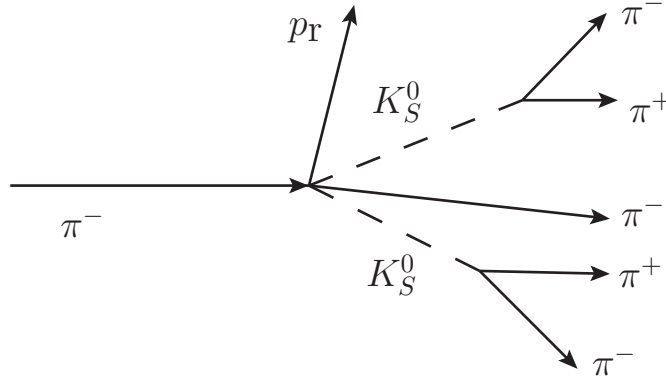


Fig. 2: Selected event topology

3.2 Event selection

The analysis so far is based on two weeks of data taken during the 2008 negative hadron beam run of the COMPASS experiment, which amounts to some 21% of the 2008 data collected with negative pion beam. These data together with 2009's will allow high-statistics partial-wave analyses. From the reconstructed data we selected events with a topology as depicted in fig. 2, i.e. one vertex with an incoming beam track and a single outgoing track, and two displaced V^0 vertices. We have not included K_S^0 s that decayed so close to the primary vertex that the reconstruction software could not separate their decay from the original interaction. This mostly affects the acceptance of slow K_S^0 s that decay close to their point of creation and we are planning to include such events should acceptance of slow K_S^0 s turn out to be an issue. We ensured that the K_S^0 s' point of origin was the primary vertex by requiring that $\cos \theta > 0.9995$ for the angle θ between the reconstructed momentum of each K_S^0 and the line connecting its decay vertex to the primary vertex. In a first selection step all events with exactly two such K_S^0 candidates with reconstructed K_S^0 mass within 5 MeV/ c^2 of the PDG value were selected.

In order to further suppress pollution from the small Kaon admixture ($O(3\%)$) in the beam we required the beam-line CEDAR detectors [11] to not have identified the beam particle as Kaon. Exclusivity was ensured by requiring the total momentum of the final state particles to be within 185 GeV and 195 GeV (nominal beam momentum 191 GeV). Additionally, we used the recoil proton detector to verify the planarity of the event, i.e. we required that the direction of the recoil proton lay in the plane formed by the beam and the total momentum of the pions (for the azimuthal angle $\Delta\phi$ between the plane of the recoil track and that of the spectrometer system: $\pi - |\Delta\phi| > 2.9$ rad). A total of 22914 events passed this selection for the reduced data set used for these preliminary studies. This already exceeds the statistics gathered by the

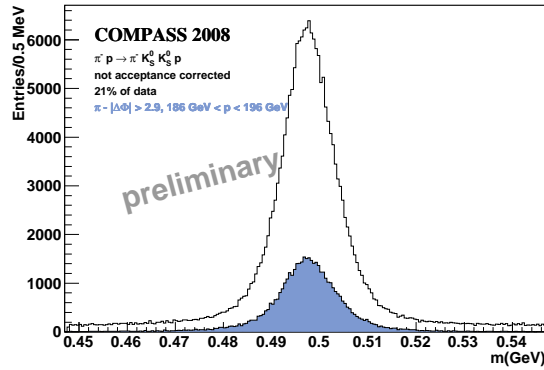


Fig. 3: Distribution of reconstructed K_S^0 masses. The upper histograms shows the distribution before requiring exclusivity as explained in the text, the filled histogram shows the final sample.

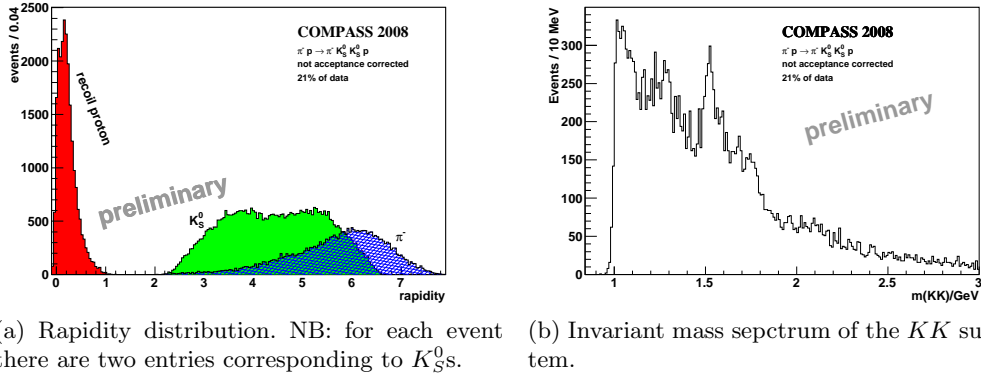


Fig. 4: Distributions illustrating the properties of the overall sample. Refer to text for selection.

WA102 collaboration [4] for their sample of centrally produced $K_S^0 K_S^0$ by approximately an order of magnitude.

As an example of the degree of purity of the selection, we show the reconstructed masses of the selected K_S^0 s in fig. 3 which shows that the final selection is both virtually free of background with a reconstructed mass nicely centered at the PDG value [12].

3.3 Kinematics of the final state

The distribution of rapidities of the particles in the selected events is depicted in fig. 4a. It shows a clear separation between the rapidity of the recoil proton and the spectrometer system. On the other hand, the rapidities of the forward particles shows no clear separation of different regimes. Overall, the pions have higher rapidity than the K_S^0 s, but there's a large fraction of overlap. On the other hand the corresponding KK mass spectrum reproduces well-known resonances fairly faithfully as show in fig. 4b.

The presence of different production processes comes apparent in fig. 5 which plots the mass of the $K\bar{K}$ system over the pion momentum. The distribution looks significantly different in the regime with low and high pion momenta. In order to suppress diffractive production where a three-body system approximately carrying the beam momentum would decay into $K_S^0 K_S^0 \pi^-$ we selected a subset where the final-state pion carries the largest momentum. Selections using rapidity gaps were also tried out, but the resulting mass spectra are comparable. The corresponding rapidity distribution and mass spectrum are depicted in fig. 6a and fig. 6b.

4 Acknowledgements

This research was supported by the DFG cluster of excellence 'Origin and Structure of the Universe' (www.universe-cluster.de).

References

1. P. Abbon, et al. (COMPASS), Nucl. Instrum. Meth. **A577**, 455 (2007), [hep-ex/0703049](#)
2. J. Bernhard, contribution in these proceedings
3. D. Barberis, et al. (WA102), Phys. Lett. **B462**, 462 (1999), [hep-ex/9907055](#)
4. D. Barberis, et al. (WA102), Phys. Lett. **B453**, 305 (1999), [hep-ex/9903042](#)
5. F. E. Close, A. Kirk, Eur. Phys. J. **C21**, 531 (2001), [hep-ph/0103173](#)
6. D. V. Bugg, Eur. Phys. J. **C52**, 55 (2007), [hep-ex/0706.1341](#)
7. E. Klempt, A. Zaitsev, Phys. Rept. **454**, 1 (2007), [hep-ph/0708.4016](#)

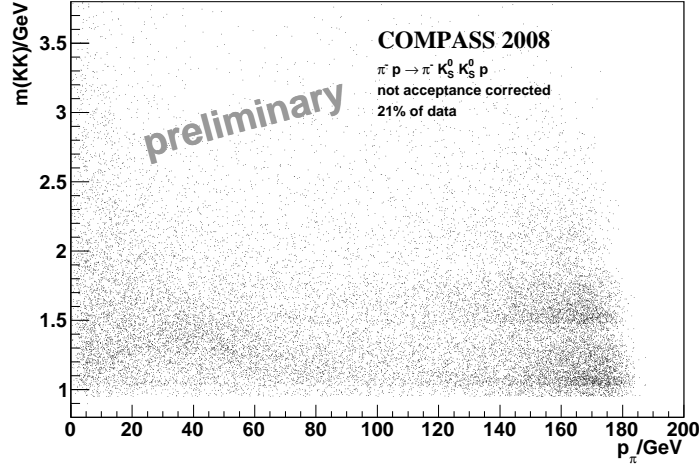
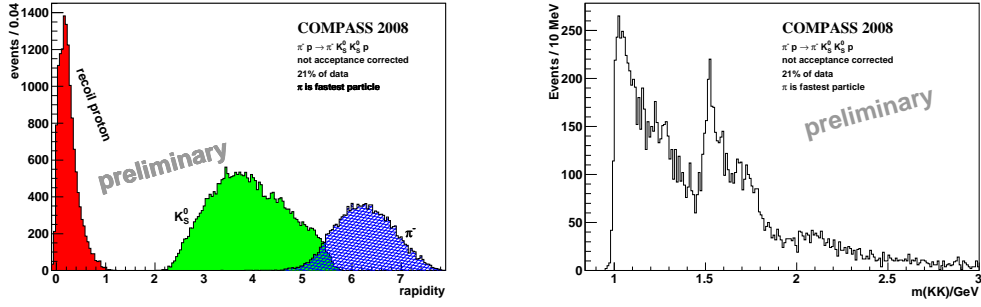


Fig. 5: Invariant mass of the $K\bar{K}$ system against the momentum of the final state π^- . The presence of different regimes is striking.



(a) Rapidity distribution. NB: for each event there are two entries corresponding to the K_S^0 s. (b) Invariant mass spectrum of the $K_S^0 K_S^0$ sub-system.

Fig. 6: Distributions illustrating the properties of the sub-sample where the pion has the highest momentum.

8. M. Chanowitz, Phys. Rev. Lett. **95**, 172001 (2005), [hep-ph/0506125](#)
9. S. U. Chung, E. Klempt, J. G. Körner, Eur. Phys. J. **A15**, 539 (2002), [hep-ph/0211100](#)
10. F. E. Close, P. R. Page, Nucl. Phys. **B443**, 233 (1995), [hep-ph/9411301](#)
11. P. Jasiński, contribution in these proceedings
12. C. Amsler, et al. (Particle Data Group), Phys. Lett. **B667**, 1 (2008)